A comparative study of the properties of yttrium and lanthanum aluminates obtained by Pechini sol–gel process

I. Carazeanu Popovici[a], A. Diacon[b], F. Moscalu[c], A. Dumbrava [a*]
[a]*Ovidius University of Constanta, Department of Chemistry and Chemical Engineering, 124 Mamaia Blvd., Constanta 900527*
[b]*University Politehnica of Bucharest, Department of Bioresources and Polymer Science, 1-7 Polizu Street, Bucharest 011061, Romania*
[c]*Ovidius University of Constanta, Department of Physics, 124 Mamaia Blvd., Constanta 900527, Romania*

The optical and photocatalytic properties of yttrium and lanthanum aluminates obtained by Pechini sol-gel process were studied by comparison. The aluminates were characterized by XRD, TEM, SEM, DRS, FTIR and PL spectroscopy. The photocatalytic properties were investigated in the removing of both cationic and anionic dyes from aqueous solutions. A higher photocatalytic activity was identified for yttrium aluminate (90% - 97% after 90 min), with the maximum value for methylene blue solution (97.15%), and a photocatalytic activity of 46.88% was determined for lanthanum aluminate in the degradation of methylene blue. The photocatalytic activity was in a good correlation with the aluminates optical behavior.

(Received January 25, 2022; Accepted April 11, 2022)

Keywords: Yttrium aluminate, Lanthanum aluminate, Optical properties, Photoluminescence, Photocatalytic activity, Wastewater treatment

1. Introduction

The transition metal aluminates are an important class of mixed oxides, mainly known for their properties like electronic, catalytic, ceramic, and luminescent. The aluminates of rare earth (RE) elements, including yttrium and lanthanum, are interesting especially for their applications in electronic devices as host matrix for laser, phosphors, scintillator, thermoluminescent detector, holographic recording medium, etc. [1, 2], but they have been less studied in photocatalytic processes. Three types of rare earth aluminates can be defined based on RE/Al ratio, namely $RE_4Al_2O_9$, $REAlO_3$, and $RE_3Al_5O_{12}$, each of them having its practical importance [3, 4]. As respects to yttrium aluminate (YAO), in the Al_2O_3–Y_2O_3 system four phases can occur, namely a Y-richer phase $Y_4Al_2O_9$ (yttrium aluminum monoclinic, YAM), an Al-richer phase $Y_3Al_5O_{12}$ (yttrium aluminum garnet, YAG), and two phases with the same stoichiometry, $YAlO_3$, that is a stabile (yttrium aluminum perovskite, YAP) and respective a metastable phase (yttrium aluminum hexagonal, YAH) which was identified during the soft chemistry routes [2, 5]. YAP is notable by a combination of luminescent and spectral-generation properties, having a high mechanical strength, hardness, heat conductivity, and transparency in a wide spectral range [6]. YAP has a distorted perovskite structure of $GdFeO_3$ type, consisting in the distorted octahedrons formed around the Al^{3+} ions by oxygen ligands, and Y^{3+} ions situated in the holes between the octahedrons, with strongly deformed polyhedrons developed by the twelve nearest oxygen ions; three different Al-O bonds and six different Y-O bonds were identified [7, 8]. The perovskite structure of lanthanum aluminate ($LaAlO_3$, LAO) can be considered as pseudocubic, and its crystals may feature a "twinning" [9]. LAO is usually used as a substrate for high temperature superconductors and ferroelectric thin films, but other utilizations have been also proposed, for example based on its antimicrobial activity and adsorption properties; the most important applications of lanthanum aluminate are typically due to its photoluminescent properties [10, 11].

* Corresponding author. adumbrava@univ-ovidius.ro
https://doi.org/10.15251/JOR.2022.182.259

The synthesis methods for RE aluminates include conventional ceramic processing routes, sol-gel, co-precipitation, calcination, spray pyrolysis, microwave assisted synthesis, flame synthesis, and alumina impregnating method [1, 2, 4, 12]. The right choice of obtaining method is important because the nature and some properties of synthesized RE aluminates depend on the synthesis route [13]. Several authors revealed that in the synthesis of YAP the achievement of single phase YAP represents a "hard challenge", being generally very difficult to suppress the parallel formation of YAG and YAM. It was demonstrated that YAG is thermodynamically favored with respect to YAP, both for the formation from oxides and for the reaction Al_2O_3 + 3YAP = YAG, and YAM is usually present as a consequence of YAG formation, due to deviation from YAP stoichiometry [14, 15]. A number of methods were proposed for the synthesis of YAP, the most known involving solid state synthesis at high temperatures (1600 ^oC). But, during the long-term action of high temperatures in the YAP synthesis, intermediate products are formed and polycrystalline ceramics with grains having large sizes, wide size distribution, and irregular structure can be obtained [6]. To avoid the inconveniences of very high temperatures, several wet chemical methods were proposed for the synthesis of yttrium aluminates, like co-precipitation spray pyrolysis, sol-gel, solvothermal synthesis, combustion synthesis, etc. [16].

Sol-gel chemistry is considered an alternative to solid-state chemistry, giving the advantage of the molecular level mixing of reagents, which offers a better control of the particle morphology and size. As a disadvantage, it was demonstrated that a homogeneous precursor at room temperature does not ensure homogeneity throughout a reaction. The Pechini method (metal-polymer gel decomposition method) was developed on the principles of sol–gel chemistry and involves the coordination of chelating ligands (such is citrate) to form a homogeneous solution of metal - citrate complexes, having the advantage of a polymeric precursor in which the metal ions are homogeneously dispersed throughout the network [17]. The process involves three stages, i.e. (i) the preparation of stable aqueous solution, (ii) the polyesterification to form a solid polymeric resin, and (iii) the decomposition/combustion of the resin to an amorphous oxide which is followed by the crystallization of the oxide phase [18]. A variety of modified Pechini methods were also used for the synthesis of rare earth aluminates, including yttrium and lanthanum aluminates, as it allows homogeneous powders to be obtained [19-25].

Hereby we studied the ability of YAO and LAO obtained by Pechini sol-gel method to be used in the wastewater treatment by determination of spectral, luminescent and photocatalytic properties. We also report the synthesis and structural characterization of YAO by Pechini sol–gel process, using citric acid as organic complexing agent and ethylene glycol.

2. Experimental

2.1. Materials

The high purity reagents were obtained from Sigma-Aldrich (yttrium oxide, Y_2O_3; aluminum nitrate, $Al(NO_3)_3 \cdot 9H_2O$; citric acid monohydrate, $HOC(COOH)(CH_2COOH)_2 \cdot H_2O$; ethylene glycol, $HOCH_2CH_2OH$; crystal violet, CV; Congo red, CR) and Merck (lanthanum(III) nitrate hexahydrate, $La(NO_3)_3 \cdot 6H_2O$; nitric acid, HNO_3; methylene blue, MB), and used as received, without further purification.

2.2. Synthesis

Yttrium aluminate. In 150 mL of 0.4 M $Al(NO_3)_3$ solution (0.06 mol $Al(NO_3)_3$) was added a solution of $Y(NO_3)_3$, previously obtained by the reaction of 6,89 g Y_2O_3 with 37 mL of 5 N HNO_3 solution diluted with 100 mL H_2O (0.06 mol $Y(NO_3)_3$). The mixture was magnetically stirred at room temperature. After 15 min, a mixture of citric acid and ethylene glycol was added in a molar ratio of 1:1, by continuing the magnetic stirring. The heterogeneous mixture obtained at room temperature was matured at 80 ^oC for 4 h and then dehydrated in an oven for 3 h at 235 ^oC, with obtaining an orange xerogel. The xerogel was pestled and heated in a program controlled electronic muffle furnace (Nabertherm, Germany) to 700, 800, 900, 1000 and 1100 ^oC, respectively at a heating rate of 0.25 ^oC/min, holding for 3 h, and then cooled down to room temperature naturally by switching off the furnace.

Lanthanum aluminate synthesis has been published elsewhere [22]. In brief, a similar procedure was followed, starting from $La(NO_3)_3 \cdot 6H_2O$ and $Al(NO_3)_3 \cdot 9H_2O$ as precursors, citric acid as ligand, and ethylene glycol.

2.3. Characterization of powders

YAO powder was investigated by X-ray diffraction (XRD) performed on a Bruker D8 X-ray diffractometer with CuK_α radiation, λ = 1.5406 Å. The 2θ range was 15 – 60° with a step size of 0.05° and a resolution of 0.01. The transmission electron microscopy (TEM) investigation of YAO powder was performed on a Philips CM 120 ST transmission electron microscope operated at 100 kV, with 2 Å resolution. The scanning electron microscopy (SEM) examination of YAO powder was performed with a JEOL JMS 5800L electron microscope; the samples were coated with gold and examined in the as fired condition, i.e., without polishing. The UV–visible diffuse reflectance spectra (DRS) of YAO and LAO powders were recorded in the range of 220 – 850 nm, on a Jasco V 550 spectrophotometer with an integrating sphere, using MgO as the reference. The photoluminescence (PL) spectra were measured on a Jasco FP-6500 spectrofluorometer. The FTIR spectra were measured by using the ATR mode on an Agilent Cary 630 FTIR spectrometer, ZnSe ATR, in the 4000 - 650 cm^{-1} domain.

2.4. Photocatalytic properties

The photocatalytic properties of YAO and LAO were tested in the degradation of organic dyes in aqueous solutions. The dyes were methylene blue (MB, 15 mg/L), crystal violet (CV, 15 mg/L), and Congo red (CR, 25 mg/L). The photocatalyst powder/ dye solution ratio was 0.05 g/ 100 mL. The procedure for the photocatalytic experiments was described in our previous studies [26-28]. Briefly, a suspension of 0.05 g powder in 100 mL aqueous dye solution (MB, CV, respectively CR) was stirred in a glass installation with a magnetic stirrer and samples were collected at regular intervals. The samples were centrifuged at 10,000 rpm for 15 min (M 815 M centrifuge from Elektro-Mag) and filtered for complete removal of catalyst particles. We simulated a visible light source by using a 45 W lamp which matching with the solar light, as confirmed by HR4000CG-UV-NIR high-resolution spectrometer, Ocean Optics. The dye degradation was monitored by the UV–Vis absorption spectra of dyes solutions recorded in the range of 200 – 900 nm, on a Jasco V 550 spectrophotometer, and was estimated by C_t/C_0 ratio, where C_t and C_0 are the concentrations of the dye at certain time, *t*, and initial concentration, respectively. The efficiency of the photocatalyst was estimated by determining the photocatalytic activity (*PA*), which has been calculated as [26, 27]:

$$PA = \frac{C_0 - C_t}{C_0} x100 = \frac{A_0 - A_t}{A_0} x100 \quad (1)$$

where A_0 and A_t are the absorbance value for CR solutions when the reaction time is 0 and *t*, respectively (based on Lambert – Beer law).

3. Results and discussion

3.1. Characterization of powders

The crystal structure and phase composition of YAO were determined by XRD. The XRD patterns of powders obtained by gel calcination at various temperatures in the range of 700 – 1100 °C are shown in Fig. 1.

It can be seen from Fig. 1 that the most intense peak in XRD pattern for all the powders is assigned to YAP, which was identified together with YAG in the YAO powder. Furthermore, the powder composition depends on the temperature and the transformations between the phases can be assumed from XRD patterns. Namely, for the sample calcined at 700 °C an almost amorphous structure can be identified. Only four very weak diffraction peaks can be observed, all of them being assigned to YAP (CIF 00-100-8923 http://www.crystallography.net/cod/1008923.html). As the temperature rises, more crystalline YAO powders were found. For the powder obtained at 800

°C, the diffraction peaks are assigned to YAP and also to YAG (CIF 00-152-9037 http://www.crystallography.net/cod/1529037.html), which appears as a crystalline phase at higher temperatures [11]. By further raising the temperature, few new peaks appeared together with an increasing intensity of all peaks assigned to YAP and YAG. The formation of both YAP and Al_2O_3 by increasing the temperature favors the reaction between them and, as consequence, the obtaining of YAG and as well of YAM to respect the system stoichiometry [14]. The fact that YAM has not been identified in XRD patterns can mean that it is obtained in small quantities and/or in an amorphous form.

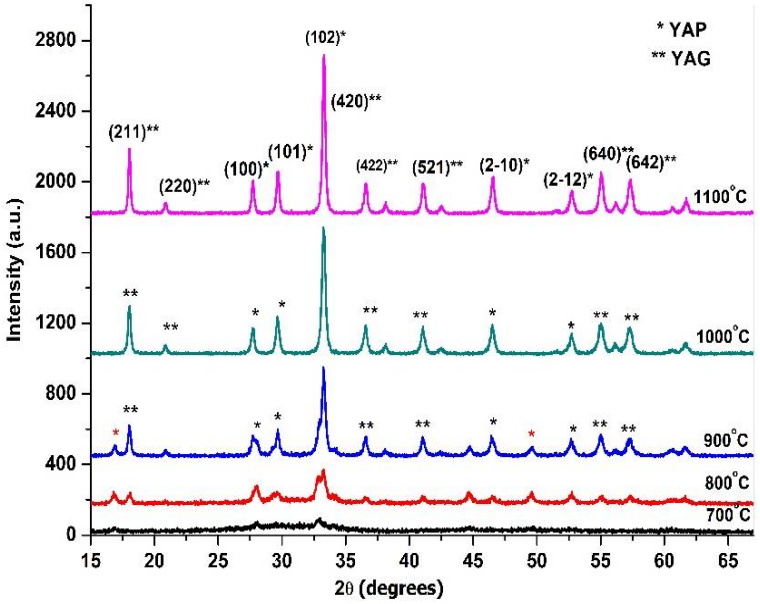

Fig. 1. XRD patterns for YAO samples.

A mixture of YAP and YAG can be identified in the final product (1100 °C). Therefore, the XRD patterns evidenced the crystallization of YAP, in a first stage, followed by the crystallization of YAG due to the partial transformation of YAP in YAG. It was demonstrated that the formation of YAG and YAM as intermediate stable phases in the synthesis of YAP is favored by the chemical inhomogeneities and large particles of amorphous precursor, as well the low heating rates, caused by the differences in the Al(III) and Y(IIII) ions mobility [2]. The formation of a mixture of yttrium aluminates in the sol-gel synthesis was also evidenced by other authors. For example, Su et al. [16] demonstrated that the phase transformation sequence during the growth of the calcination temperature depends on the molar ratio of reagents. It deserves to be noted that a single phase of $LaAlO_3$ was obtained in the synthesis of LAO by a similar procedure [22].

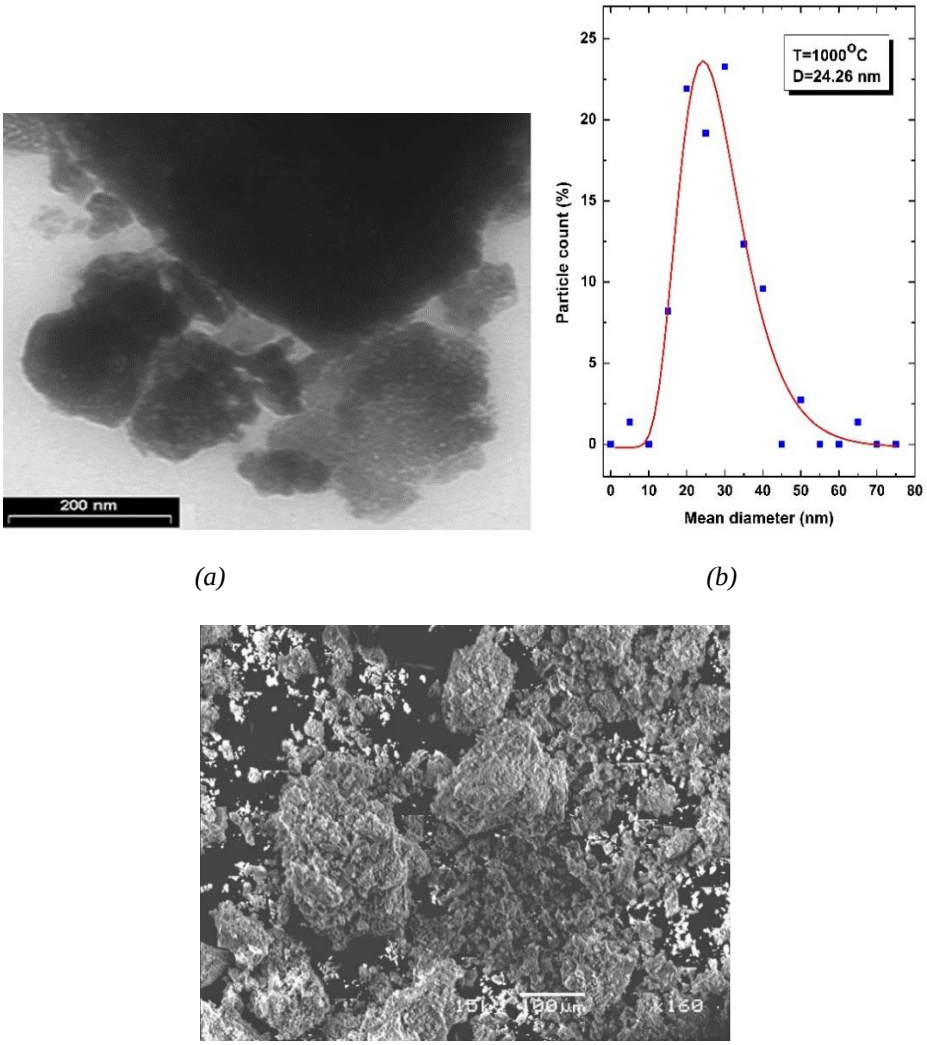

(a) *(b)*

(c)

Fig. 2. YAO powder morphology: TEM image (a); particle size distribution histogram from TEM (b); SEM image (c).

The morphology of as-obtained YAO powder was analyzed by TEM and SEM. The TEM image (Fig. 2.a) demonstrated that the nanoparticles of powder are agglomerated in larger aggregates. The calculated mean dimension of particles is 24.26 nm (Fig. 2.b). The SEM image confirmed the presence of large aggregates which appear to be porous, and also a mixture of particles with different morphology, i.e. YAP and YAG.

The electronic spectra of YAO and LAO are presented in Fig. 3.a. Although both maxima of absorption are shifted to higher values of wavelength for YAO in comparison with LAO, the shape of spectra is quite similar, but adsorption bands are more intense for LAO. The main absorption bands can be assigned to the transition of electrons from the valence to conduction band. Having in view the YAP band structure determined by calculations [7], which revealed that the top of the valence band is formed by the unbound states of oxide ions, the core of valence band is mainly formed by 2*s* orbitals of O^{2-} mixed with 4*p* levels of Y^{3+}, and the bottom of the conduction band is mostly formed by 4*d* and 5*s* orbitals of Y^{3+}, it is considered that the $YAlO_3$ band gap is mainly determined by the interaction Y–O rather than Al–O. The 3*d* orbitals of Al^{3+} form deeper levels in the conduction band, and $2p$ (O^{2-}) → $4d$ + $5s$ (Y^{3+}) transitions are most probable [8]. A shoulder at about 400 nm for both samples, but more intense for LAO, can be assigned to a charge transfer transition and is responsible for the light yellowish color of the

powder. The weak band situated in the YAO spectrum in visible domain (479 nm), which is missing in the LAO spectrum, can be assigned to the impurities which can form isolated levels in the YAO band gap [8]. The position of maxima in the electronic spectra can be corelated with the band gap energy and the particles dimension.

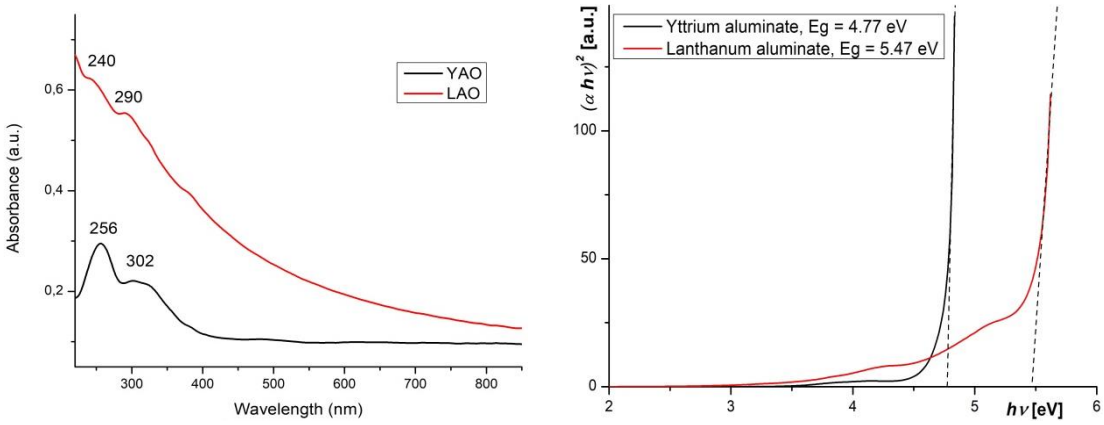

(a) *(b)*

Fig. 3. UV-vis spectra of YAO and LAO powders (a); Tauc plots for YAO and LAO powders (b).

The optical band gap energy (*E*g) was calculated from the UV-vis DRS by using Tauc equation (Fig. 3.b) [27-31]. Since the band gap energy of a semiconductor depicts the energy needed to excite an electron from the valence band to the conduction band, the determination of the band gap energy is important in predicting the photochemical properties of semiconductors [31]. As it can be seen in Fig. 3.b, a wider band was determined for LAO, accordingly being expected a lower photocatalytic activity for this nanopowder. The calculated value of E_g for YAO (4.77 eV) is comparable but lower than the value of 4.99 eV estimated by Ching and Xu [7] for a $YAlO_3$ crystal. The narrower band for YAO can be corelated with the supplementary energy levels due to the YAG impurities. The value calculated for LAO (5.47 eV) is comparable with some other experimental calculations reported by various groups within the range 5.5–6.55 eV [32].

The emission properties of the aluminate powders were investigated by PL spectroscopy. The PL emission spectra of YAO and LAO samples for excitation wavelengths in UV and visible domain are displayed in Fig. 4. It can be seen that the shape and the bands position in the emission spectra depend strongly on the excitation wavelength. This feature can be attributed to differences in the depth of penetration of exciting radiation at different wavelengths, as the microcrystalline structure close to the surface may vary with depth [33].

Two emissions, i.e. excitonic and trapped photoluminescence, are generally observed in PL spectra of semiconductor materials. The excitonic emission is sharp and found near the absorption edge, while the trapped emission is broad and found at a longer wavelength [34, 35]. For $YAlO_3$ it was stated that the formation of excitons with holes self-trapped at unbound 2*p* orbitals of O^{2-} oxygen and the occurrence of luminescence due to the recombination annihilation of the holes with electrons of the conduction band are expected, based on electronic spectra and calculated band structure, at energy values closed to the energy of $O^{2-} \rightarrow Y^{3+}$ transition. Various models were proposed to explain the nature of the UV intrinsic luminescence of YAP [8]. Under the excitation with 290 nm, the emission sharp band is centered at 304 nm, very close to the adsorption edge (302 nm for YAO, respective 290 nm for LAO). Actually, the sharp band is a part of a pair of intrinsic luminescence bands which were also reported by other authors [8], its pair being mostly out of the spectrometer range. The existence of the pair of bands is more obvious under the excitation of 290 nm (Fig. 4.a). It can be seen that under a UV excitation the emission intensity is higher for YAO than for LAO. Under the excitation with 395 nm wavelength radiation, a sharp band situated at 411 nm was evidenced for YAO, respective at 418 nm for LAO. The emission broad band under 290 nm excitation is situated in 350 – 500 nm domain, resulting by the

overlapping of two other broad bands with few maxima. Under 395 nm excitation, the emission sharp band for LAO is partially overlapped with the broad band, which is centered at 467 nm. In this case, the shape of spectra is different for the two aluminates. By comparing the spectra of the studied nanopowders, it can be observed that the shape of the spectra is very similar under 290 nm excitation, with a higher intensity for YAO, but quite different under the 395 and 445 nm excitations. The blue emission of LAO sample (Fig. 4.b) is composed of several peaks at 419, 449, 462 and 467 nm, respectively. The weaker blue emission of YAO sample is also composed of a few peaks at 449, 462, 467, 472, 480 and 491 nm, respectively. A similar observation is correct for the emission spectra from Fig. 4.a in the blue domain. It was demonstrated that the mechanism of such emissions in the blue domain should be associated with the defects or impurities, which act as trapped states within the band gap [36-38]. The bands situated in green – yellow region (520 – 590 nm) occur at excitation with higher wavelength radiation (445 and 520 nm) and are more intense for LAO (at 520 nm, respective 546 nm). They may have several explanations including donor-acceptor pairs, surface localized states, defects related to stoichiometry, and structural defects [38].

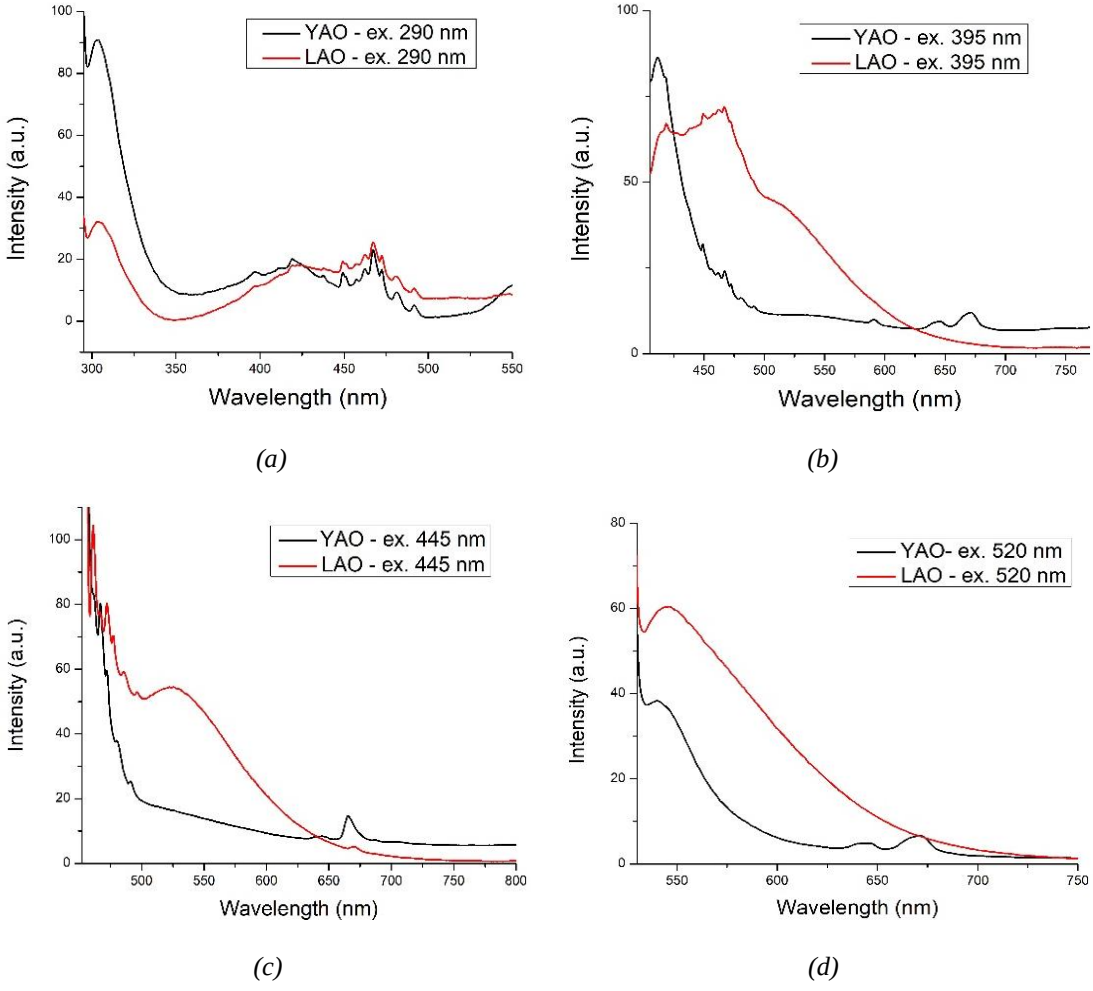

Fig. 4. The PL spectra of YAO and LAO, using excitation wavelengths of 290 (a), 395 (b), 445 (c) and 520 (d) nm.

The higher intensity of PL spectrum for YAO in UV, respective for LAO in visible domain can be associated with a higher recombination rate, respective a lower separation rate of photo-induced charge carriers, which can be correlated with the photocatalytic activity [39]. In addition to the charges recombination, it was shown that the luminescence properties depend on interfacial processes, which can occur at the boundary between the particles and the surrounding

medium, and are influenced by the synthesis procedure [39]. Having in view that in our study the synthesis procedure was similar for both nanopowders, we consider that the photocatalytic activity can be corelated mainly with the charge recombination process. Indeed, by using as light source a lamp which matches the solar spectrum, a lower photocatalytic activity was determined for LAO in comparison with YAO, which is in concordance with the broad and intense emission of LAO sample in visible domain (Fig. 4.b-d).

The FTIR-ATR spectra of YAO and LAO nanopowders are displayed in Fig. 5.

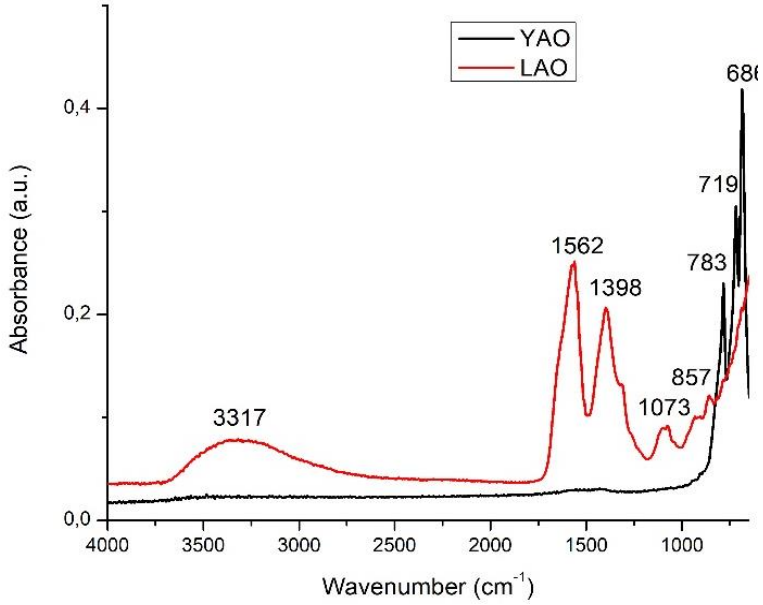

Fig. 5. FTIR-ATR spectra of YAO and LAO samples.

In the YAO spectrum can be found three peaks, at 783, 719 and 686 cm^{-1}, which can be assigned to the metal-O vibrations [40, 41]. There is no evidence for water molecules or for residues from processing steps in the YAO powder. Several peaks can be identified in the LAO spectrum. The intense peaks situated at 1562 and 1398 cm^{-1} can be assigned to C–O vibrations of the stretching type, which are associated with the complex (La/Al) – O – C – O – (La/Al) that was identified in LAO by other authors [24]. The ascendent shape of the spectrum is due to the vibrational bans at 650 cm^{-1} characterizing the vibration of the system (La/Al) – O, with the AlO_6 and the LaO_{12} structures. Another peak assigned to these structures is expected to appear outside the studied domain, around 440 cm^{-1} [24]. The weak bands found in FTIR spectrum can be assigned to precursors that have not been burned. The broad band in the 3800 – 2800 cm^{-1} can be assigned to the O-H stretching vibration water and absorbed water [25]. This band is absent in YAO spectrum, indicating a higher hydrophilicity for LAO compared to YAO.

3.2. Photocatalytic properties

The photocatalytic properties of aluminates were tested in the degradation of the aqueous solutions of three organic dyes, with different charge and structure. It was demonstrated that both the charge and structure of a dye are able to influence the interaction between the dye and the photocatalyst surface, especially their adsorption onto the catalyst surface as the first step in the heterogenous catalytic process. The three dyes are MB and CV, cationic dyes with different molecular structure, and CR anionic dye. The MB structure is linear, and the charge is located in the center of the molecule. The CV molecular structure is an equilateral triangle and the charge is located on the vertex angle [42]. Due to its negative charge, the CR anion has the ability to coordinate at the cations on the catalyst surface. The absorbance of dye solution was measured as a function of irradiation time at 663 nm for MB (the band assigned to MB as monomer, MB^+) [43], 585 nm for CV [44], and 497 nm [26] for CR (as indicative of azo bond degradation).

We first tested the photocatalytic properties of YAO. The discoloration of solutions in photocatalytic process (Fig. 6) was estimated by C_t/C_0 ratio and the photocatalytic degradation curves are presented in Fig. 7. A high photocatalytic activity can be observed in the degradation of all three dyes.

The rapid discoloration of solutions over YAO, proven by the electronic spectra of solutions, is an argument for the high adsorption capacity of YAO powder. After only 60 min the dyes were almost complete removed from solutions, the values of PA being 96.37% for MB, 95.59% for CV, and 86.77% for CR. The lowest value for CR can be correlated with its negative charge, but also with its higher initial concentration.

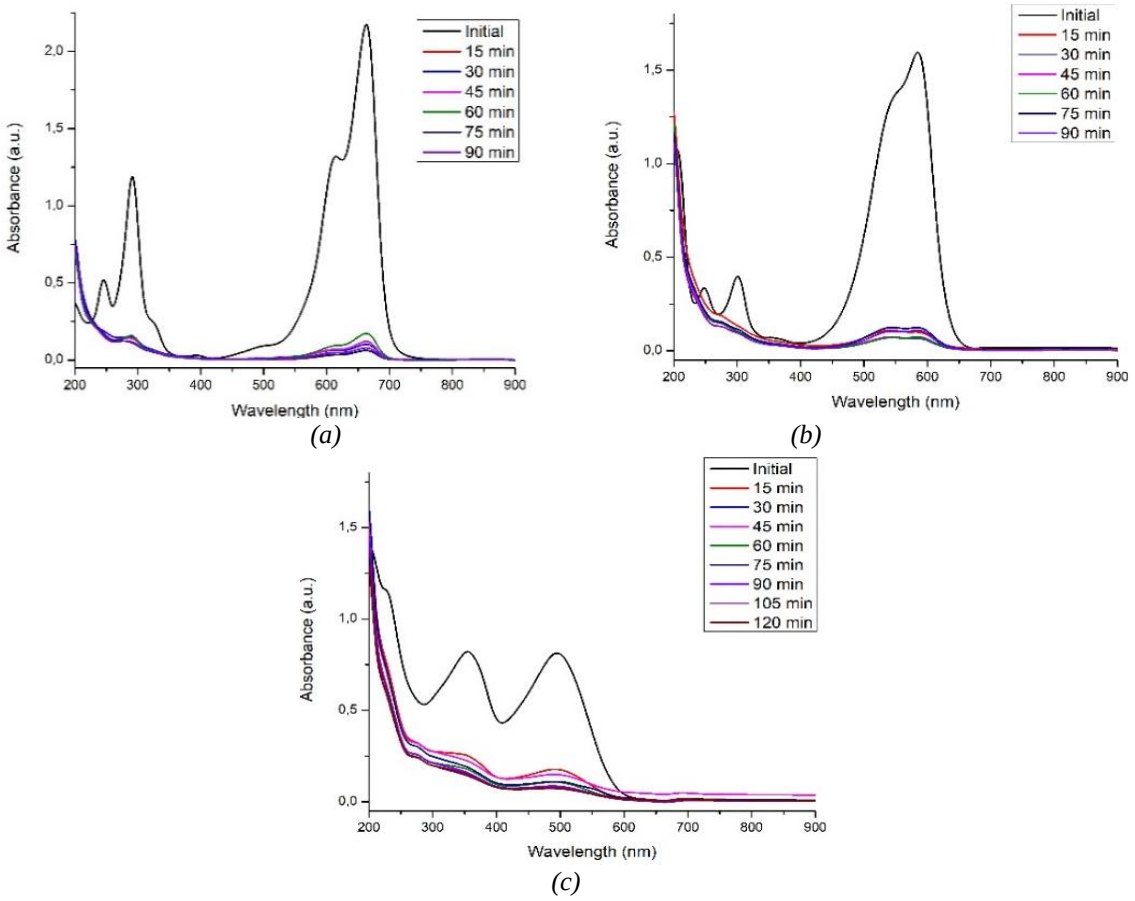

Figure 6. The UV–Vis spectral changes of MB (a), CV (b), and CR (c) solutions over YAO as function of time.

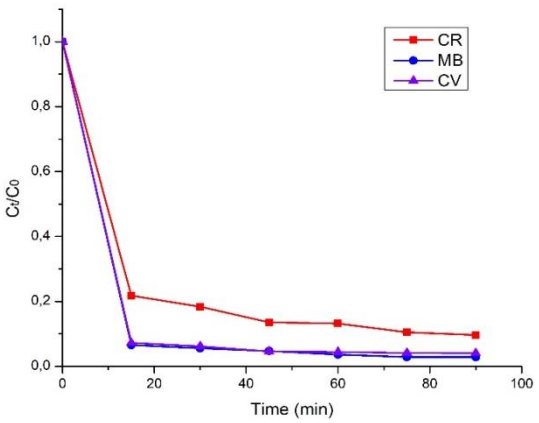

Fig. 7. The photocatalytic degradation curves of CR, MB and CV over YAO.

We tested the photocatalytic properties of LAO powder in the degradation of the cationic dyes, for which the best results in degradation over YAO were obtained. The initial variation of dye concentration is lower in comparison with the solution discoloration onto YAO, meaning a lower adsorption of the dye onto LAO surface in comparison with YAO (Fig. 8). The subsequent variation of dye concentration is also low, showing a lower photocatalytic activity. After 60 min the PA values are 39.90% for MB and 44.50% for CV (Fig. 9).

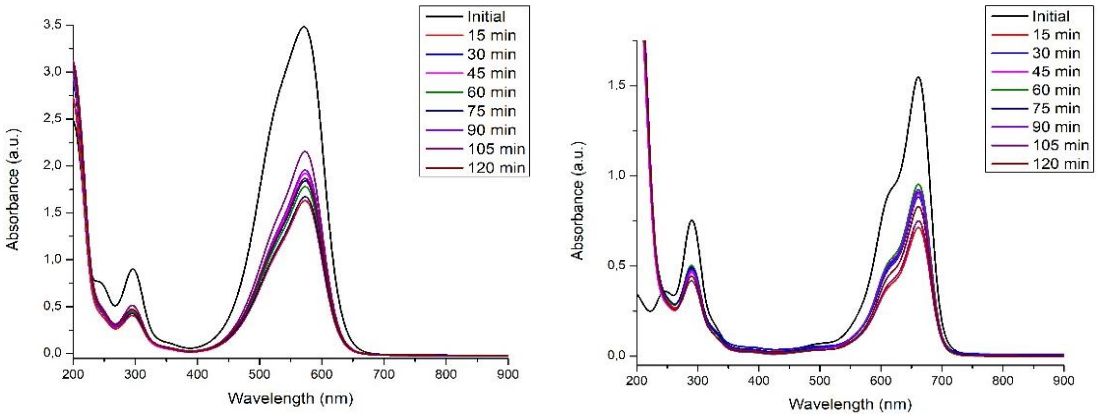

Fig. 8. The UV–Vis spectral changes of MB (a) and CV (b) solutions over LAO as function of time.

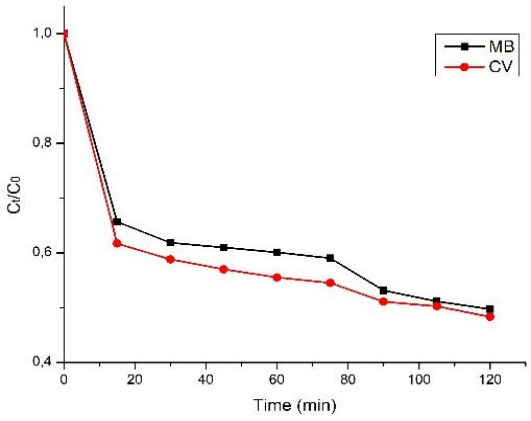

Fig. 9. The photocatalytic degradation curves of MB and CV over LAO.

On the basis of photoluminescence properties, a higher photocatalytic activity was expected for YAO in comparison with LAO. In addition, an important contribution had the adsorption process, corelated with the discoloration of solution, and thus the powder morphology. A mean diameter of 24.26 nm was determined for yttrium aluminate nanopowder, lower in comparison with lanthanum aluminate nanopowder with a mean diameter of 37.54 nm. The presence of YAG as impurities in YAO powder, with the appearance of new energy levels that lead to the narrowing of the bandgap energy, and therefore a larger band gap for LAO of 5.47 eV in comparison with 4.77 eV for YAO is another argument for YAO higher photocatalytic activity.

4. Conclusions

We studied the spectral, luminescent and photocatalytic properties of YAO and LAO obtained by Pechini sol-gel method in order to be used in the wastewater treatment. The optical

properties were analyzed by using DRS and PL spectroscopy, and an optical band gap energy of 4.77 eV for YAO, respective 5.47 eV for LAO, was determined from Tauc equation. The photoluminescence spectroscopy revealed a more intense emission for YAO in comparison with LAO in UV, but a higher intensity and broader emission for LAO in the visible domain. The FTIR spectra confirmed the synthesis of aluminates. The characterization of YAO powder by XRD demonstrated the presence of YAG as an impurity, which represents an usual problem in the YAP synthesis, as other authors have communicated. However, unlike the obtaining of YAP for other applications, its use as a photocatalyst is not disadvantaged by the presence of YAG. On the contrary, the impurities can generate new electronic levels which improve the nanopowers interaction with the light together with the photocatalytic properties. A high photocatalytic activity was determined for YAP in the degradation of both cationic and anionic dyes. For LAO nanopowder, which was obtained as a single phase $LaAlO_3$, a lower photocatalytic activity (around 50%) was determined in the degradation of cationic dyes. Our study demonstrated that YAP, even more so when it is impurified with YAG, can be used successfully in removing the dyes from wastewater.

References

[1] K. Byrappa, M. Yoshimura, Hydrothermal Synthesis of Native Elements and Simple Oxides. In "Handbook of Hydrothermal Technology", Second Edition, Elsevier Inc. 2013, pp. 569-614; https://doi.org/10.1016/C2009-0-20354-0

[2] J.F. Carvalho, F.S. De Vicente, S. Pairis, P. Odier, A.C. Hernandes, A. Ibanez, Synthesis of YAP nanopowder by a soft chemistry route, Journal of the European Ceramic Society 29, 2511-2515 (2009); https://doi.org/10.1016/j.jeurceramsoc.2009.03.005

[3] T. Takeda, K. Kato, S. Kikkawa, Gel combustion synthesis of rare earth aluminate using glycine or urea, Journal of Ceramic Society of Japan 115, 588-591(2007); https://doi.org/10.2109/jcersj2.115.588

[4] S. Kasala, M.V.S. Doss, Microwave assisted synthesis and powder flowability characteristics of rare-earth aluminate (ReAlO3, Re = La, Gd, Nd, Y) powders, Transactions of the Indian Ceramic Society 78, 13-19. (2019); https://doi.org/10.1080/0371750X.2019.1566024

[5] L. Nadaraia, N. Jalabadze, R. Chedia, L. Khundadze, Production of nanopowder and bulk aluminate ceramic scintillators, Ceramics International 39, 2207-2214 (2013); https://doi.org/10.1016/j.ceramint.2012.09.018

[6]. T.F. Kuznetsova, A.I. Rat'ko, E.V. Bolotnikova, E.N. Poddenezhnyi, Synthesis of mesoporous precursors of yttrium aluminate with the perovskite structure, Colloid Journal 68, 457-461 (2006); https://doi.org/10.1134/S1061933X06040090

[7]. W.Y. Ching, Y.N. Xu, Nonscalability and nontransferability in the electronic properties of the Y-Al-O system, Physical Review B 59, 12815-12821 (1999); https://doi.org/10.1103/PhysRevB.59.12815

[8]. Yu.V. Zorenko, A.S. Voloshinovskii, G.M. Stryganyuk, I.V. Konstankevych, Ultraviolet luminescence of single crystals and single-crystal films of YAlO3, Optics and Spectroscopy 96, 70-76 (2004); https://doi.org/10.1134/1.1643988

[9]. Y.G. Makeev, A.P. Motornenko, N.T. Cherpak, I.P. Babiichuk, M.B. Kosmyna, On the anisotropy of dielectric permittivity in single crystal lanthanum aluminate substrates, Technical Physics Letters 28, 221-223 (2002); https://doi.org/10.1134/1.1467281

[10]. C.R. Manjunatha, B.M. Nagabhushana, M.S. Raghu, S. Pratibha, N. Dhananjaya, Anjana Narayana Perovskite lanthanum aluminate nanoparticles applications in antimicrobial activity, adsorptive removal of Direct Blue 53 dye and fluoride, Materials Science & Engineering C 101, 674-685 (2019); https://doi.org/10.1016/j.msec.2019.04.013

[11]. T. Rivera-Montalvo, A. Morales-Hernandez, A.A. Barrera-Angeles, R. Alvarez-Romero, C. Falcony, J. Zarate-Medina, Modified Pechini's method to prepare LaAlO3:RE thermoluminescent materials, Radiation Physics and Chemistry 140, 68-73 (2017); https://doi.org/10.1016/j.radphyschem.2017.01.022

[12]. A.O. Merkushkin, Rare-earth aluminate based ceramic, Glass and Ceramics 69, 321-323

(2013); https://doi.org/10.1007/s10717-013-9470-4
[13]. S.Y. Cho, I.T. Kim, K.S. Hong, Microwave dielectric properties and applications of rare-earth aluminates, Journal of Materials Research 14, 114-119(1999); https://doi.org/10.1557/JMR.1999.0018
[14]. M. Blosi, S. Albonetti, M. Dondi, A.L. Costa. M. Ardit, G. Cruciani, Sol-gel combustion synthesis of chromium doped yttrium aluminum perovskites, Journal of Sol-Gel Science and Technology 50, 449-455 (2009); https://doi.org/10.1007/s10971-009-1906-5
[15]. O. Fabrichnaya, H.J. Seifert, F. Ludwig, F. Aldinger, A. Navrotsky, The assessment of thermodynamic parameters in the Al2O3-Y2O3 system and phase relations in the Y-Al-O system, Scandinavian Journal of Metallurgy 30, 175-183 (2001); https://doi.org/10.1034/j.1600-0692.2001.300308.x
[16]. X. Su, J. Zhou, G. Bai, J. Zhang, P. Zhao, Low temperature synthesis and characterization of YAG nanopowders by polyacrylamide gel method, Ceramics International 42, 17497-17502 (2016); https://doi.org/10.1016/j.ceramint.2016.08.058
[17]. A.E. Danks, S.R. Hall, Z. Schnepp, The evolution of 'sol-gel' chemistry as a technique for materials synthesis, Materials Horizons 3, 91-112 (2016); https://doi.org/10.1039/C5MH00260E
[18]. T.O.L. Sunde, T. Grande, M.A. Einarsrud, Modified Pechini synthesis of oxide powders and thin films. In: Klein L., Aparicio M., Jitianu A. (eds), Handbook of Sol-Gel Science and Technology, Springer, Cham. (2016); https://doi.org/10.1007/978-3-319-19454-7_130-1
[19]. I. Carazeanu Popovici, E. Chirila, V. Popescu, V. Ciupina, G. Prodan, Sol-gel preparation and characterization of perovskite lanthanum lithium titanate, Journal of Materials Science 42, 3373-3377 (2007); https://doi.org/10.1007/s10853-006-0683-6
[20]. Y. Xu, G. Huang, H. Long, Synthesis of lanthanum aluminate via the ethylenediaminetetraacetic acid gel route, Ceramics International 29, 837-840 (2003); https://doi.org/10.1016/S0272-8842(03)00026-9
[21]. D.V. Mamonova, I.E. Kolesnikov, A.A. Manshina, M.D. Mikhailov, V.M. Smirnov, Modified Pechini method for the synthesis of weakly-agglomerated nanocrystalline yttrium aluminum garnet (YAG) powders, Materials Chemistry and Physics 189, 245-251 (2017); https://doi.org/10.1016/j.matchemphys.2016.12.025
[22]. I. Carazeanu Popovici, V. Ciupina, G. Prodan, M.A. Gîrţu, Structural characterisation of lanthanum aluminate synthetized by the Pechini method, J. Optoelectron. Adv. M. 10, 2942 - 2946 (2008).
[23]. M.K. Cinibulk, Synthesis of yttrium aluminum garnet from a mixed-metal citrate precursor, Journal of American Ceramic Society 83, 1276-1278 (2000); https://doi.org/10.1111/j.1151-2916.2000.tb01367.x
[24]. I.S. Silveira, N.S. Ferreira, D.N. Souza, Structural, morphological and vibrational properties of LaAlO3 nanocrystals produced by four different methods, Ceramics International 47, 27748-27758 (2021); https://doi.org/10.1016/j.ceramint.2021.06.201
[25] R. Marin, G. Sponchia, P. Riello, R. Sulcis, F. Enrichi, Photoluminescence properties of YAG: Ce3+, Pr3+ phosphors synthesized via the Pechini method for white LEDs, Journal of Nanoparticle Research 14, 886 (2012); https://doi.org/10.1007/s11051-012-0886-5
[26] A. Dumbrava, G. Prodan, D. Berger, M. Bica, Properties of PEG-capped CdS nanopowders synthesized under very mild conditions, Powder Technology 270, 197-204 (2015); https://doi.org/10.1016/j.powtec.2014.10.012
[27] A. Dumbrava, D. Berger, G. Prodan, F. Moscalu, A. Diacon, Facile synthesis, characterization and application of functionalized cadmium sulfide nanopowders, Materials Chemistry and Physics 173, 70-77 (2016); https://doi.org/10.1016/j.matchemphys.2016.01.040
[28] I. Carazeanu Popovici, G. Stroie, G. Voicu, F. Moscalu, A. Diacon, A. Dumbrava, A comparison between alkaline earth metal titanates for application as photocatalysts in wastewater treatment, Desalination and Water Treatment 98, 115 - 122 (2017); https://doi.org/10.5004/dwt.2017.21706
[29] J. Tauc, R. Grigorovici, A. Vancu, Optical properties and electronic structure of amorphous germanium, Physica Status Solidi B 15, 627-637 (1966); https://doi.org/10.1002/pssb.19660150224

[30] A.R. Zanatta, Revisiting the optical bandgap of semiconductors and the proposal of a unified methodology to its determination, Scientific Reports 9, 11225 (2019); https://doi.org/10.1038/s41598-019-47670-y

[31] P. Makuła, M. Pacia, W. Macyk, How to correctly determine the band gap energy of modified semiconductor photocatalysts based on UV−Vis spectra, The Journal of Physical Chemistry Letters 9, 6814−6817 (2018); https://doi.org/10.1021/acs.jpclett.8b02892

[32] M. Rizwan, S. Gul, T. Iqbal, U. Mushtaq, M.H. Farooq, M. Farman, R. Bibi, M. Ijaz, A review on perovskite lanthanum aluminate (LaAlO3), its properties and applications, Materials Research Express 6, 112001 (2019); https://doi.org/10.1088/2053-1591/ab4629

[33] A. Weinreb, Vacuum ultraviolet excited luminescence of organic systems: a review. In: "Organic Scintillators and Scintillation Counting", Academic Press 1971; https://doi.org/10.1016/B978-0-12-356250-0.50006-3

[34] A. Dumbrava, D. Berger, G. Prodan, C. Matei, F. Moscalu, A. Diacon, The influence of Triton X-100 surfactant on the morphology and properties of zinc sulfide nanoparticles for applications in azo dyes degradation, Materials Chemistry and Physics 193, 316 (2017); https://doi.org/10.1016/j.matchemphys.2017.02.040

[35] S. Kakarndee, S. Juabrum, S. Nanan, Low temperature synthesis, characterization and photoluminescence study of plate-like ZnS, Materials Letters 164, 198-201 (2016); https://doi.org/10.1016/j.matlet.2015.10.154

[36] L.E. Muresan, M. Ayvacikli, J. Garcia Guinea, A. Canimoglu, Y. Karabulut, N. Can, Preparation and characterization of yttrium based luminescence phosphors, Optical Materials 74, 150-158 (2017); https://doi.org/10.1016/j.optmat.2017.01.044

[37] L. Shi, F. Wang, Y. Wang, D. Wang, B. Zhao, L. Zhang, D. Zhao, D. Shen, Photoluminescence and photocatalytic properties of rhombohedral CuGaO2 nanoplates, Scientific Reports 6, 21135 (2016); https://doi.org/10.1038/srep21135

[38] S. Repp, E. Erdem, Controlling the exciton energy of zinc oxide (ZnO) quantum dots by changing the confinement conditions, Spectrochimica Acta Part A: Molecular and Biomolecular Spectroscopy 152, 637-644 (2016); https://doi.org/10.1016/j.saa.2015.01.110

[39] J. Liqiang, Q. Yichun, W. Baiqi, L. Shudan, J. Baojiang, Y. Libin, F. Wei, Fu Honggang, S. Jiazhong, Review of photoluminescence performance of nano-sized semiconductor materials and its relationships with photocatalytic activity, Solar Energy Materials and Solar Cells 90, 1773-1787 (2006); https://doi.org/10.1016/j.solmat.2005.11.007

[40] K. Laishram, R. Mann, N. Malhan, R.K. Gupta, Studies of process parameters on scale up of Nd:YAG nanopowder synthesis by sol-gel process, Defence Science Journal 62, 198-201 (2012); https://doi.org/10.14429/dsj.62.837

[41] A.M. Hofmeister, K.R. Campbell, Infrared spectroscopy of yttrium alluminum, yttrium gallium, and yttrium iron garnets, J. Appt. Phys. 72, 638-646 (1992); https://doi.org/10.1063/1.351846

[42] X. Yu, C. Wei, H. Wu, Effect of molecular structure on the adsorption behavior of cationic dyes onto natural vermiculite, Separation and Purification Technology 156, 489-495 (2015); https://doi.org/10.1016/j.seppur.2015.10.039

[43] J. Cenens, R.A. Schoonheydt, Visible spectroscopy of methylene blue on hectorite, laponite b, and barasym in aqueous suspension, Clays and Clay Minerals 36, 214-224 (1988); https://doi.org/10.1346/CCMN.1988.0360302

[44]. S. Mohanty, S. Moulick, S.K. Maji, Adsorption/photodegradation of crystal violet (basic dye) from aqueous solution by hydrothermally synthesized titanate nanotube (TNT), Journal of Water Process Engineering 37, 101428 (2020); https://doi.org/10.1016/j.jwpe.2020.101428